in vivo *33*: 567-572 (2019)
doi:10.21873/invivo.11512

Infrared and Raman Spectroscopic Studies of Molecular Disorders in Skin Cancer

JANE ANASTASSOPOULOU[1], MARIA KYRIAKIDOU[1], EFTHYMIA MALESIOU[1], MICHAEL RALLIS[2] and THEOPHILE THEOPHANIDES[1]

[1]*Radiation Chemistry and Biospectroscopy, Chemical Engineering School, National Technical University of Athens, Athens, Greece;*
[2]*Department of Pharmacy School of Health Sciences, National and Kapodistrian University of Athens, Athens, Greece*

Abstract. *Aim: To investigate the molecular structural disorders of cancerous skin. Materials and Methods: Human malignant melanoma and basal cell carcinoma biopsies were used for the investigation. Fourier transform infrared (FT-IR), Raman spectroscopy, and scanning electron microscopy were utilized. Spectral differences between healthy, basal cell carcinoma and melanoma tissues were recorded. Results: The FT-IR bands of $\nu_{as}CH_2$, ν_sCH_2 and Raman ν_sCH_3 of cell membrane lipids were increased in intensity in melanoma due to an increased lipophilic environment. The FT-IR band at 1,744 cm^{-1} assigned to malondialdehyde can be used as a band diagnostic of cancer progression. The amide I bands at 1,654 cm^{-1} and 1,650 cm^{-1} for Raman and FT-IR, respectively were broader in spectra from melanoma, reflecting changes of protein secondary structure from α-helix to β-sheet and random coil. The intensity of the FT-IR band at 1,046 cm^{-1} was increased in melanoma, suggesting glycosylation of the skin upon cancer development. Another band that might be considered as diagnostic was found at about 815 cm^{-1} in melanoma and was attributed to Z-DNA configuration. As far as we know, this is the first time that scanning electron microscopy revealed that metal components of titanium alloys from tooth implants were transferred to melanoma tissue taken from the back of one patient. Conclusion: Vibrational spectroscopy highlighted increased glycosylation in melanoma.*

Correspondence to: Emeritus Professor Theophile Theophanides, National Technical University of Athens, Chemical Engineering School, Radiation Chemistry and Biospectroscopy, Zografou Campus, 15780 Athens, Greece. Mobile: +30 6936993712, e-mail: theo.theophanides@gmail.com

Key Words: Skin cancer, infrared spectroscopy, Raman spectroscopy, bio-corrosion, metal implant.

Although skin cancer affects all types of skin, it is more common in less pigmented individuals, and the incidence is growing every year globally (1, 2). Sun exposure is a cause of skin alteration that can lead to cancer (3-6). Basal-cell carcinoma (BCC) and squamous-cell carcinoma (SCC) are the most common non-melanoma skin cancer types, while malignant melanoma (MM) is the most aggressive and is responsible for almost all deaths from skin cancer (1-3).

Vibrational spectroscopies [infrared (IR) absorption and Raman scattering] have gained great attention from the medical community as interesting tools for the non-invasive (non-destructive) characterization and identification of the molecular features of cancer tissues (7-10). IR spectroscopy is based on the changes of dipole moment of molecules during their interaction with the IR radiation (11, 12), while Raman is based on the change of electric polarizability of the molecules (13, 14). Both methods reveal information not only on the characteristic functional groups, such as CH, NH OH, C-O-C and PO_2^- of lipid chains, proteins, glycans, DNA, but also on the changes of the surrounding environment induced by disease (8-19).

In the present research work, Fourier transform (FT-IR) and Raman spectroscopies in combination with scanning electron microscopy (SEM) were used to study the molecular and conformational changes induced by BCC and MM in human skin.

Materials and Methods

Patients. For the present study, eight biopsies of BCC from the head and cheek, and nine biopsies of MM from the back of patients (age 58-70 years) were used as they were histologically characterized. For normal skin tissue, adjacent healthy tissue in the region of the biopsy was used. The size of the biopsies of the patients did not allow us to separate the epidermal layers. The size of biopsies was 50 μm to 1 mm. All biopsies were fixed in buffered formaldehyde solutions immediately after surgical excision. In order to obtain the spectra, the samples were not fixed in paraffin, since the removal

of paraffin by solvents also removes soluble products produced during the disease, thus losing valuable information. Based on our experience using solvents such as hexane or dimethylsulfoxide to remove paraffin, also removes products such as aldehydes and glycan end-products, which are produced during cancer development and prefer a more lipophilic environment (7-10). The samples were then washed with distilled water and dehydrated under vacuum at room temperature.

Statement of Ethics. The samples were taken according to Helsinki rules and the Greek law of ethics for *ex vivo* clinical research studies.

Attenuated total reflection (ATR)-FT-IR spectroscopy. The IR spectra were recorded with a Nicolet 6700 spectrometer (Thermo Scientific, Waltham, MA, USA). With the ATR-FT-IR technique, the samples were not homogenized. In ATR technique, the infrared light passing through the crystal is reflected many times into the sample thereby amplifying the signal. We have seen that for soft tissues, the depth of the sample must be 10 μm, while for bones a size of 5 μm was enough to give good spectra. This allows us to obtain spectra from small samples and to change the sites of the same tissues of each patient. In order to minimize the signal-to-noise ratio, each spectrum consisted of 120 co-added spectra at a spectral resolution of 4 cm^{-1}. OMNIC 7.2a workstation software (Thermo Scientific, Waltham, MA, USA) was used for data analysis.

Raman spectroscopy. The Raman spectra were recorded by using a micro-Raman spectrometer Invia confocal microscope (Renishaw, UK), with excitation at 785 nm and power at 145 mW. Raman scattering was measured throughout with sequential 10 s integration time and microscope objective magnification of ×20. The excitation at 785 nm was more suitable for the skin tissue specimens since the received spectra did not show any auto-fluoresce.

SEM. The detection of skin surface and architecture morphology were carried out using a scanning electron microscope (Fei Co, the Netherlands). SEM was combined with energy dispersive X-ray (EDX) apparatus for analysis of the elemental composition in different sites of the tissues. It must be noted that there was not any coating of the samples with carbon or gold.

Results and Discussion

Figures 1 and 2 show the FT-IR and Raman superimposed spectra, respectively, of normal skin, BCC and MM. In both techniques, the recording spectra of BCC and MM revealed significant changes in intensities and frequency shifts of the absorption bands in comparison with the normal tissues. The spectral region of 4,000-3,000 cm^{-1} represents absorption bands due to the stretching vibrations of *v*OH and *v*NH groups of glycosaminoglycans, a key component of skin, proteins and collagen of the skin, as well as the stretching vibration bands of water molecules in the cells (20, 21). These bands are not shown in Raman spectra, as can be seen in Figure 2, because they were too weak. The broad band at about 3,484 cm^{-1} in the spectra of normal tissues is assigned to the stretching vibration of *v*OH groups of water molecules, and to *v*OH of polysaccharides of hyaluronic acid, which is also a key component of skin. The band decreases in intensity in FT-IR spectra of both BCC and MM, reflecting the dehydration of skin in both cancer types.

The strongest band in FT-IR spectra at 3,287 cm^{-1} is assigned to stretching vibration of NH groups of proteins in A conformation. This band decreased from normal skin to BCC and MM, indicating damage to protein peptide bonds. The band appearing at about 3,062 cm^{-1} indicates that some of the proteins have the configuration of amide B. In the case of amide B, the β-sheet protein structure predominates (22). This means that the effect of the NH group of the peptide bond -NHCO- is stronger than that of C=O, unlike amide A, where the effect of C=O is stronger. The coexistence of both A and B conformations of proteins illustrates the prevalence of different hydrogen bonds in length and strength that hold the protein strands together (20, 22). Hydrogen bonding is important in stabilizing the protein helix and any change implies that the physiological environment has been changed. We have found that these changes are very important and constitute a basic criterion in order to characterize the disease and its progression stage (8-12, 20, 21).

The bands in the spectral region between 3,000 to 2,870 cm^{-1} are assigned to symmetric and antisymmetric stretching vibrations of methyl and methylene groups of lipids, proteins and glycosides (20, 21). A considerable increase in the intensity of the symmetric stretching vibration band of νCH_2 at 2,852 cm^{-1} in MM and less in BCC was observed, while the symmetric stretching vibration band of vsCH3 at 2,958 cm^{-1} was decreased in FT-IR spectra. This finding was also obtained in colorectal (23), breast (7, 24), bone (8, 9, 21) cancerous tissues, indicating structural and conformation puckering of membranes, which in the case of cancer has changed with the surrounding medium becoming more lipophilic (9-10). Deconvolution of this region showed a new band at 2,892 cm^{-1}, which is assigned to the presence of branched alkyl chains. Based on that, it is suggested that during the disease, metabolic pathways or oxidative stress produce free hydroxyl radicals (HO•), which by reacting with lipid chains lead to alkyl free radicals and then to radical–radical reactions to form stable products. In Raman spectra, the changes due to cancer formation are more obvious in the spectral region 3,050-2,800 cm^{-1} (Figure 2). Evidence of cancer development is the increase in intensity of the band at 3,010 cm^{-1}, which is attributed to stretching vibration of olefinic v(=CH) mode. This band is also observed in FT-IR spectra of MM (Figure 1, spectrum c) concerning the involvement of oxidative stress during cancer development (19-21). The band of stretching vibration of $\nu_s CH_3$ at 2,926 cm^{-1} in spectra from normal tissues shifts to 2,936 cm^{-1} in both BCC and MM, with a parallel increase of their intensity, indicating the increase of polarizability of terminal CH_3 groups. On the contrary, the asymmetric

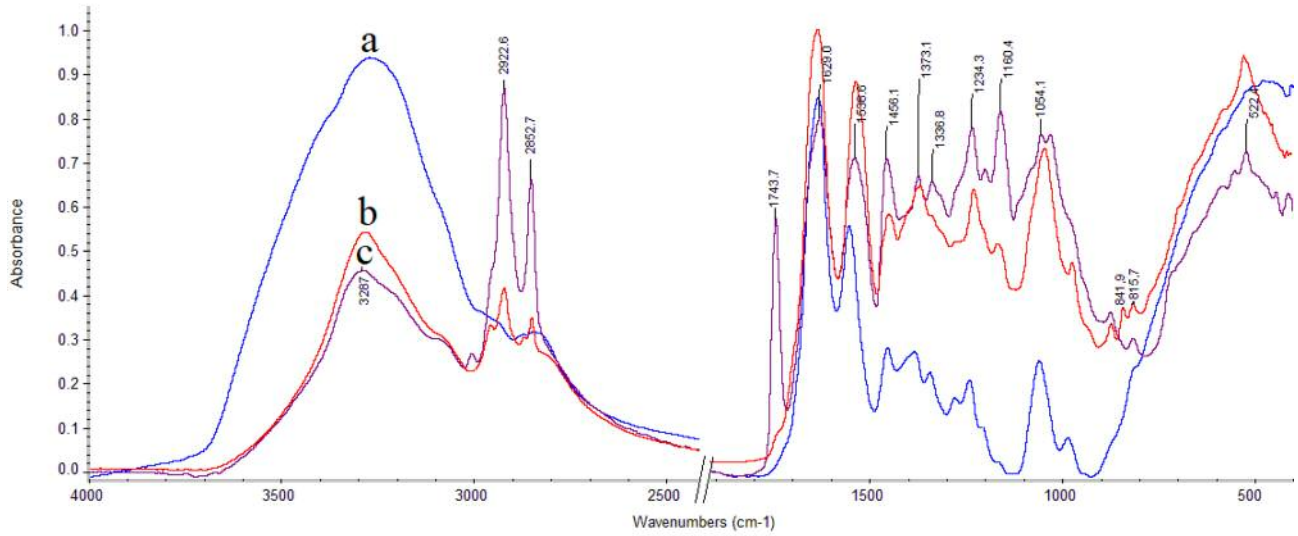

Figure 1. *Representative Fourier transform infrared spectra of skin tissues: (a-blue) normal, (b-red) basal cell carcinoma and (c-violet) melanoma in the region 4,000-500 cm^{-1}.*

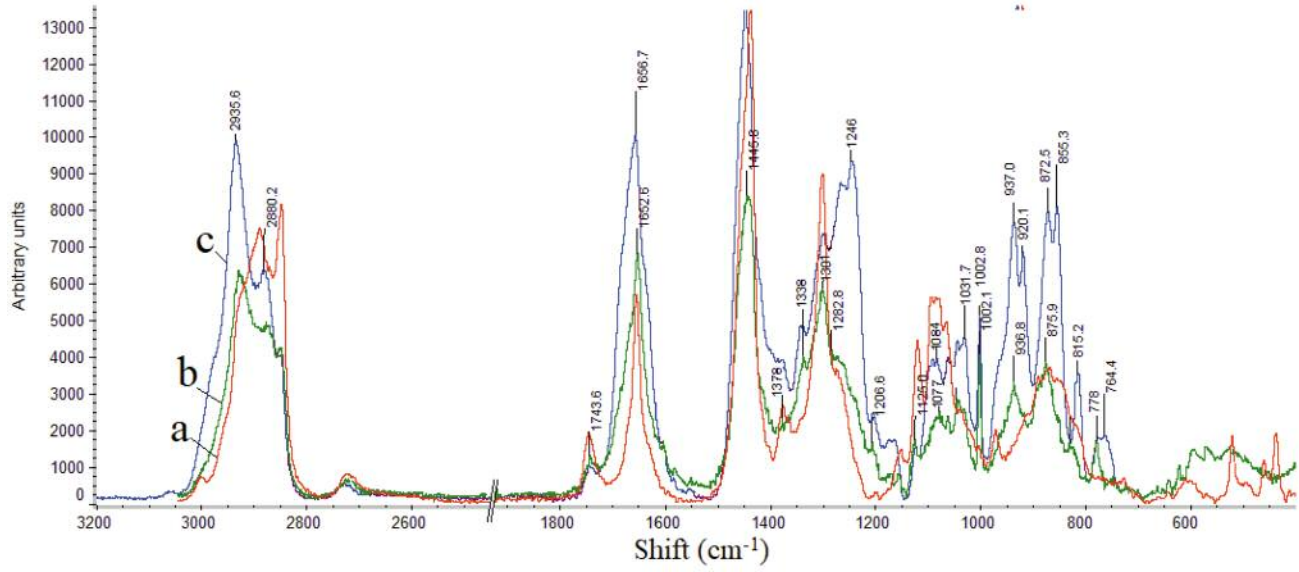

Figure 2. *Representative Raman spectra of skin tissues: (a-red) normal, (b-green) basal cell carcinoma and (c-blue) melanoma, in the region 3,200-500 cm^{-1}.*

vibration of $\nu_{as}CH_3$ at 2,960 cm^{-1} decreases considerably in intensity in spectra of both BCC and MM. The stretching vibration of asymmetric methylene $\nu_{as}CH_2$ in normal tissue from 2,880 cm^{-1} shifts to higher frequency at 2,890 cm^{-1} with a decrease in intensity. These results suggest that the hydrophobic interaction between the hydrocarbon chains as well as between intermembrane proteins changed their order-disorder puckering (16). A shift to higher frequencies of the bending vibration δCH_2 from 1,436 to 1,448 cm^{-1} was also observed in Raman spectra of MM.

The spectral region 1,800-700 cm^{-1} contains information about the secondary structure of proteins. A new high-intensity band at 1,744 cm^{-1} in FT-IR spectra of MM, appeared as a shoulder in BCC. This new band is assigned to the aldehyde group (-CHO) and is associated with lipid peroxidation (8-10, 17). The increase in intensity of this band

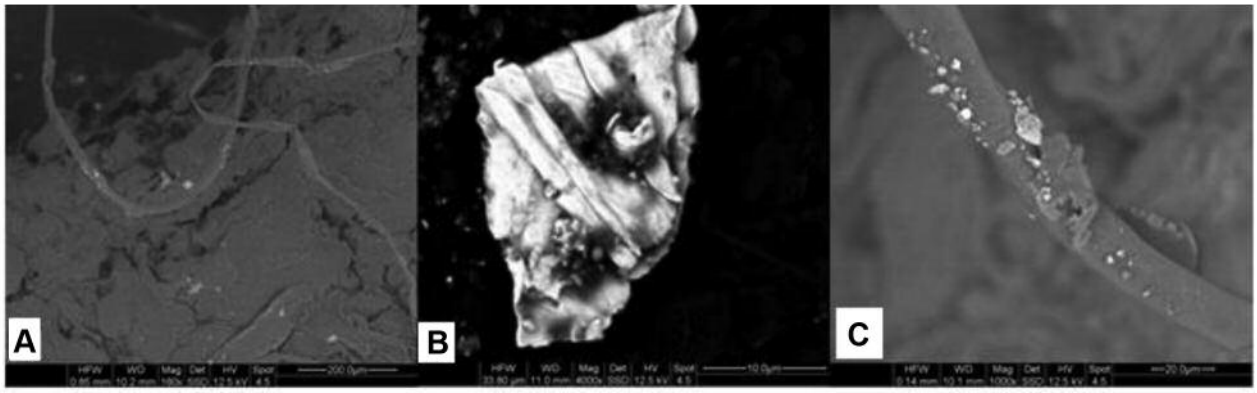

Figure 3. *Scanning electron microscopy images showing the morphology of melanoma malignant from a patient who according to clinical history had titanium alloy tooth implants. A: Misfolded proteins (×160, scale 200 μm). B: Titanium-alloy deposit encapsulated by proteins (×4000, scale 10 μm). C: Mineral deposition aggregates on the surface of protein.*

was related to disease progression. This band is not observed in Raman spectra appearing only as a shoulder, as shown in Figure 2. The high intensity FT-IR band at 1,650 cm^{-1} is assigned to *ν*C=O of amide I of the peptide bond (-NHCO-) of proteins (7-12, 22-26) and is a 'marker band' for α-helical peptide bond. This band is split upon deconvolution into three bands at 1,690 cm^{-1}, 1,650 cm^{-1} and 1,633 cm^{-1} due to the presence of a β-sheet (↓↑, anti-parallel structure), α-helix and random coil protein structure, respectively for MM, indicating that the secondary structure of proteins changed from α-helix to β-sheet and random coil upon cancer formation. Nevertheless, the bands at 1,690 cm^{-1} in combination with the band at 3,062 cm^{-1} are very characteristic of β-sheet formation and amyloid protein identification (17, 19). The appearance of the β-sheet proteins, in combination with the observed increased intensity of νCH_2 bands suggests amyloid protein formation and that the existing environment of membranes is a more ordered lipophilic environment that promotes the formation of aggregates leading finally to fibril formation.

The next intense infrared band at about 1,550 cm^{-1} is assigned to the vibration of amide II group of proteins, which is mainly due to *ν*C-N and δNH out-of-plane and the band is attributed to the β-turns of the protein and suggests that the collagen helix has an α-helix configuration. In the Raman spectra, the amide II band is not observed at all, only that of amide I, which might be due to the fact that the –NH bending vibration is not active in Raman scattering. This band in FT-IR spectra is also shifted to lower frequencies, at 1,540 cm^{-1} for MM and 1,533 cm^{-1} for BCC, upon the disease development, indicating the presence of a β-sheet (↑↑, parallel structure) conformation of proteins. The presence in the spectra of both antiparallel and parallel β-sheet conformation of proteins confirms the formation of aggregates due to the lipophilic environment as indicated from the absorption spectra in the region 3,000-2,850 cm^{-1}. Alteration of the lipophilic environment during skin carcinogenesis was also observed as reflected by increasing skin concentration of lipophilic low molecular weight antioxidants (6, 26-28) in comparison with healthy skin. Although the band of amide III in the region 1,350-1,200 cm^{-1} is not sensitive, in the spectra of MM, the bands at 1,230 cm^{-1} in IR and 1,246 cm^{-1} in Raman are associated with β-sheet structure as a result of the disease (28, 29).

Noticeable changes can also be observed in the spectral region of 1,250-1,000 cm^{-1}, where the absorption vibrational modes of the membrane groups -PO_2^{2-}, -C-O-C- and -O-C-C are found, in which an oxygen atom is linked to two carbon atoms of the sugar moiety of glycosaminoglycans together with the exocyclic -C-O-C- inter-molecule groups. The bands between 1,150 and 1,165 cm^{-1} are assigned to –C-O-C- band of sugar rings and the band at 1079 cm^{-1} to exocyclic –C-O-C- (oxygen bridge) (30, 31). The intensity of the band at 1,160 cm^{-1} was increased considerably in MM spectra, indicating the high rate of glycosylation that takes place during melanoma development. Glycosylation was also shown in other cancer types, such as breast, colon and metastatic bone cancer (7, 18, 20). This latter band can be used as a biomarker band to discriminate BCC from MM. The absorption bands at 1,046 cm^{-1} and 1,033 cm^{-1} in FT-IR and Raman spectra, respectively, assigned to *ν*C-OH of D-glucose, are also related to the increase of glycosylation upon cancer development.

The spectral region 900-800 cm^{-1} reveals information on the configuration of the sugar-phosphate groups of DNA backbone. The absorption bands at 841 cm^{-1} and 845 cm^{-1} in FT-IR and Raman spectra, respectively, originate from the sugar-phosphate of DNA backbone and are assigned to B-

DNA (32-34). These bands are not observed in the MM spectra. On the contrary, a band at 816 and 815 cm^{-1} in FT-IR and Raman spectra, respectively, is observed which is attributed to sugar-phosphate groups of DNA arising from the conformational changes of B-DNA to cancerous Z-DNA conformation (32-34). In BCC spectra both B-DNA and Z-DNA configurations coexisted (10). The high intensity band at 873 cm^{-1} is attributed to tyrosine amino acid, which is known as the base of melanin production. The intensity of this band is reduced in FT-IR spectra of MM, while in Raman it is observed at 872 cm^{-1} and is more pronounced.

SEM-EDX analysis of melanoma. Figure 3A illustrates the architecture of the surface of melanoma tissues obtained with SEM. Damaged proteins are clearly visible, in agreement with the observed spectroscopic data, as mentioned above. By increasing SEM analysis up to magnification of ×4,000 and scale 10 μm (Figure 3B), one well-lit area with the dimensions of about 17 μm and 30 μm in width and height was detected. SEM-EDX elementary analysis showed that this area was rich in titanium. According to the clinical history the patient had seven tooth implants made from titanium (Ti) alloys. It is interesting to note that in the attempt by the immune system to protect the skin from exogenous factors, it encapsulated the metal with proteins as shown in Figure 3B.

EDX detected the presence of titanium (Ti), iron (Fe), aluminum (Al), nickel (Ni) and tungsten (W). The above metals are known to be components of Ti alloys for tooth implants. Fe, Ti, W and Ni are transition metals, which under oxidative stress can induce Fenton or Haber–Weiss-like reactions, leading to excess production of hydroxyl radicals (HO•), which can interact with biological molecules leading to significant damage. From the SEM-EDX results, it is also concluded that redox reactions, which take place during metabolic activity of the patient, changed the oxidation state of the implant, which led to bio-corrosion of the Ti alloys and to an accumulation of the metals at a great distance from the site of implant. Bio-corrosion of the implant and transformation of components far from the implantation site has also been observed in carotid and aortic arteries, as well as in metastatic bone cancer (35).

Conclusion

Based on the vibrational spectroscopic data, it is concluded that cancer affects the structure of the skin at a molecular level. The increase of the absorption band intensities of methyl and methylene groups of alkyl chains demonstrates that the local environment of cancerous skin becomes more lipophilic as the cancer progresses. The new high intensity band at 1,744 cm^{-1} appears to be a diagnostic band for oxidative stress, inflammation and disease formation. In addition, the intensity of the characteristic bands at 1,046 and 1,033 cm^{-1} in FT-IR and Raman spectra are related to glycosylation of the skin upon melanoma development.

References

1 Ferlay J, Steliarova-Foucher E, Lortet-Tieulent J, Rosso S, Coebergh WW, Comber H, Forman D and Bray F: Cancer incidence and mortality patterns in Europe: Estimates for 40 countries in 2012. Eur J Cancer *49*: 1374-1403, 2013.

2 Leiter U, Eigentler T, Carbe C: Epidemiology of skin cancer. Adv Exp Med Biol *810*: 120-140, 2014.

3 Delinassios GJ, Karbaschi M, Cooke MS and Young AR: Vitamin E inhibits the UVAI induction of "light" and "dark" cyclobutane pyrimidine dimers and oxidatively generated DNA damage, in keratinocytes. Sci Rep *8(1)*: 423, 2018.

4 Grammenandi K, Kyriazi M, Katsarou-Katsari A, Papadopoulos O, Anastassopoulou J, Papaioannou GTh, Sagriotis A, Rallis M and Maibach HI: Low molecular weight hydrophilic and lipophilic antioxidants in non melanoma skin carcinomas and adjacent normal like skin. Skin Pharmacol Physiol *29*: 324-331, 2016.

5 Khalesi M, Whiteman DC, Tran B, Kimlin MG, Olsen CM and Neale RE: A meta-analysis of pigmentary characteristics, sun sensitivity, freckling and melanocytic nevi and risk of basal cell carcinoma of the skin. Cancer Epidemiol *37*: 534-543, 2013.

6 Raasch B, Maclennan R, Wronski I and Robertson I: Body site-specific incidence of basal and squamous cell carcinoma in an exposed population, Townsville, Australia. Mutat Res *422*: 101-106, 1998.

7 Anastassopoulou J, Boukaki E, Conti C, Ferraris P, Giorgini E, Rubini C, Sabbatini S, Theophanides T, Tosi G: Microimaging FT-IR spectroscopy on pathological breast tissues. Vibrat Spectr *51*: 270-275, 2009.

8 Anastassopoulou J, Kyriakidou M, Kyriazis S, Dritsa V and Kormas T: Protein folding and cancer. Anticancer Res *34*: 5806-5709, 2014.

9 Anastassopoulou J, Kyriakidou M, Kyriazis S, Kormas T, Mavrogenis AF, Dritsa V, Kolovou P and Theophanides T: An FT-IR spectroscopic study of metastatic cancerous bone. *In*: Infrared Spectroscopy-Anharmonicity of Biomolecules, Crosslinking of Biopolymers, Food Quality and Medical Applications. Theophanides T (ed.). IntechOpen, pp. 89-100, 2015.

10 Kyriakidou M, Anastassopoulou J, Tsakiris A, Koui M and Theophanides T: FT-IR spectroscopy study in early diagnosis of skin cancer. In Vivo *31*: 1131-1137, 2017.

11 Theophanides T and Anastassopoulou J: Infrared spectroscopy applied to cancer studies. Anticancer Res *34*: 6204-6206, 2014.

12 Theophanides T: Infrared Spectroscopy-Life and Biomedical Science. IntechOpen, 2012. doi: 10.5772/2655.

13 Larkin PJ: Infrared and Raman Spectroscopy. Principles and Spectral Interpretation. Elsevier, Amsterdam, the Netherlands, 2017.

14 Yeagle PL: The Structure of Biological Membranes, Third Edition. CRC Press, 2012.

15 Megaloikonomos P, Panagopoulos G,N, Bami M, Igoumenou VG, Dimopoulos L, Milonaki A, Kyriakidou M, Mitsiokapa E Anastassopoulou J and Mavrogenis AF: Harvesting, isolation and differentiation of rat adipose-derived stem cells. Curr Pharm Biotechnol *19*: 19-29, 2018.

16 Yoshida S and Koike K: Lipid and Membrane dynamics in biological tissues-Infrared spectroscopic studies. Advance in Planar Lipid Bilayers and Liposomes. Elsevier Inc. VoI 13, pp. 1-32, 2011.
17 Kotoulas C, Mamarelis I, Koutoulakis E, Kyriakidou M, Mamareli V, Tanis O, Malesiou E, Theophanides T and Anastassopoulou J: The influence of diabetes on atherosclerosis and amyloid fibril formation of coronary arteries. A FT-IR spectroscopic study. Hell J Atheroscler *8*: 15-29, 2017.
18 Conti C, Ferraris P, Giorgini E, Rubini C, Sabbatini S, Tosi G, Anastassopoulou J, Arapantoni P, Boukaki E, Theophanides T and Valavanis C: FT-IR microimaging spectroscopy: discrimination between healthy and neoplastic human colon tissues. J Mol Struc *881*: 46-51, 2008.
19 Brancaleon L, Bamberg MP, Sakamaki T and Kollias N: Attenuated total reflection-Fourier transform infrared spectroscopy as a possible method to investigate biophysical parameters of stratum corneum *in vivo*. J Invest Dermatol 116: 380-386, 2001.
20 Kyriakidou M, Mavrogenis AF, Kyriazis S, Markouizou A, Theophanides T and Anastassopoulou J: An FT-IR spectral analysis of the effects of γ-radiation on normal and cancerous cartilage. In Vivo *30*: 599-604, 2016.
21 Mavrogenis A, Kyriakidou M, Kyriazis S and Anastassopoulou J: Fourier transform infrared spectroscopic studies of radiation-induced molecular changes in bone and cartilage. Expert Rev Qual Life Cancer Care *1*: 459-469, 2016.
22 Barth A and Zscherp C: What vibrations tell us about proteins. Quarterly Rev Biophys *35(4)*: 369-430, 2002.
23 Rigas B, Morgello S, Goldman IS and Wong PT: Human colorectal cancers display abnormal Fourier-transform infrared spectra. Proc Natl Acad Sci USA *87*: 8140-8144, 1990.
24 Dukor RK: Vibrational Spectroscopy in the Detection of Cancer. *In*: Handbook of Vibrational Spectroscopy. Chalmers JM and Griffiths PR (eds.) John Wiley and Sons Ltd., VoI 5, pp. 3335-3361, 2002.
25 Maiti NC, Apetri MM, Zagorski MG, Carey PR and Anderson VE: Raman spectroscopic characterization of secondary structure in natively unfolded proteins: r-Synuclein. J Am Chem Soc *126*: 2399-2408, 2004.
26 Cai S and Singh BR: Identification of β-turn and random coil amide III infrared bands for secondary structure estimation of proteins. Biophys Chem *80*: 7-20, 1999.
27 Shindo Y, Witt E, Han D, Epstein W and Packer L: Enzymic and non-enzymic antioxidants in epidermis and dermis of human skin. J Invest Dermatol *102*: 122-124, 1994.
28 Kohen R, Oron M, Zelkowicz A, Kanevsky E, Farfouri S and Wormser U: Low molecular weight antioxidants released from the skin's epidermal layers: an age-dependent phenomenon in the rat. Exp Gerontol *39*: 67-72, 2004.
29 Eikje NS, Aizawa K and Ozaki Y: Vibrational spectroscopy for molecular characterization and diagnosis; premalignant and malignant skin tumors. Biotechnol Annu Rev *11*: 191-225, 2005.
30 Varelas X, Bouchie MP and Kukuruzinska MA: Protein *N*-glycosylation in oral cancer: Dysregulated cellular networks among DPAGT1, E-cadherin adhesion and canonical Wnt signaling. Glycobiology *24(7)*: 579-591, 2014.
31 Bansil R, Yannas IV and Stanlay HE: Raman spectroscopy: A structural probe of glycosaminoglycans. Biochim Biophys Acta *541*: 536-542, 1978.
32 Theophanides T and Tajmir-Riahi HA: Flexibility of DNA and RNA upon binding to different metal cations. An investigation of the B to A to Z conformational transition by Fourier transform infrared spectroscopy. J. Biomol Struct Dynamics *2*: 995-1004, 1985.
33 Theophanides T and Tajmir-Riahi HA: FT-IR spectroscopic evidence of C2'-endo, anti, C3'-endo, anti, sugar ring pucker in 5'-GMP and 5'-IMP nucleotides and their metal-adducts. *In*: Structure and Motion: Membrane, Nucleic Acids & Proteins, Clementi G, Gorongiu M, Sarma E and Sarma RH (eds). ISBN Adenine Press, New York, pp. 521-530, 1985.
34 Tajmir-Riahi HA and Theophanides T: An FT-IR study of DNA and RNA conformational transitions at low temperatures J Biomol Struct Dynamics *3*: 537-542, 1985.
35 Mamarelis I, Pissaridi K, Dritsa V, Kotileas P, Tsiligiris V, Tzilalis V and Anastassopoulou J: Oxidative stress and atherogenesis: An FT-IR spectroscopic study. In Vivo *24*: 883-888, 2010.

Received November 5, 2018
Revised November 29, 2018
Accepted December 7, 2018